Spin-lattice dynamics model with angular momentum transfer for canonical and microcanonical ensembles

Mara Strungaru,[1] Matthew O A Ellis,[2] Sergiu Ruta,[3] Oksana Chubykalo-Fesenko,[4] Richard F L Evans,[1] and Roy W Chantrell[1]

[1]*Department of Physics, University of York, York, United Kingdom*
[2]*Department of Computer Science, University of Sheffield, Sheffield, United Kingdom*
[3]*Department of Physics,University of York, York, United Kingdom*
[4]*Instituto de Ciencia de Materiales de Madrid, CSIC, Madrid, Spain*

A unified model of molecular and atomistic spin dynamics is presented enabling simulations both in micro-canonical and canonical ensembles without the necessity of additional phenomenological spin damping. Transfer of energy and angular momentum between the lattice and the spin systems is achieved by a phenomenological coupling term representing the spin-orbit interaction. The characteristic spectra of the spin and phonon systems are analyzed for different coupling strength and temperatures. The spin spectral density shows magnon modes together with the uncorrelated noise induced by the coupling to the lattice. The effective damping parameter is investigated showing an increase with both coupling strength and temperature. The model paves the way to understanding magnetic relaxation processes beyond the phenomenological approach of the Gilbert damping and the dynamics of the energy transfer between lattice and spins.

I. INTRODUCTION

With the emergent field of ultrafast magnetisation dynamics[1] understanding the flow of energy and angular momentum between electrons, spins and phonons is crucial for the interpretation of the wide range of observed phenomena[2–5]. For example, phonons strongly pumped in the THz regime by laser excitation can modulate the exchange field and manipulate the magnetisation as shown for the magnetic insulator YIG [6] or in Gd[7]. The excitation of THz phonons leads to a magnetic response with the same frequency in Gd[7], proving the necessity of considering the dynamics of both lattice and spins. Phonon excitations can modulate both anisotropy and exchange which can successfully manipulate [8–10] or potentially switch the magnetisation [11,12], ultimately leading to the development of low-dissipative memories.

Magnetisation relaxation is typically modeled using the phenomenological description of damping proposed by Landau and Lifshitz[13] and later Gilbert[14], where the precessional equation of motion is augmented by a friction-like term, resulting in the Landau-Lifshitz-Gilbert (LLG) equation. This represents the coupling of the magnetic modes (given primarily by the localised atomic spin) with the non-magnetic modes (lattice vibrations and electron orbits). The LLG equation and its generalisations can be deduced from the quantum-mechanical approaches assuming an equilibrium phonon bath and the weak coupling of the spin to the bath degrees of freedom[15–17]. Thus the standard approach works on the supposition that the time scales between the environmental degrees of freedom and the magnetic degrees of freedom are well separated and reducing the coupling between the magnetization and its environment to a single phenomenological damping parameter[18,19]. In reality, the lattice and magnetisation dynamics have comparable time-scales, where the interaction between the two subsystems represents a source of damping, hence the necessity of treating spin and lattice dynamics in a self-consistent way.

To investigate these phenomena, and aiming at predictive power for the design of competitive ultrafast magnetic nano-devices, advanced frameworks beyond conventional micromagnetics and atomistic spin dynamics[20] are needed[21]. A complete description of magnetic systems includes the interaction between several degrees of freedom, such as lattice, spins and electrons, modeled in a self-consistent simulation framework. The characteristic relaxation timescales of electrons are much smaller ($\approx$ fs) in comparison to spin and lattice ($100\,\text{fs} - \text{ps}$), hence magnetisation relaxation processes can be described via coupled spin and lattice dynamics, termed Spin-Lattice Dynamics (SLD) [22–29]. SLD models can be crucial in disentangling the interplay between these sub-systems. Spin-lattice coupling has recently been studied via first-principle methods. Fransson *et al.*[30] demonstrated the possible symmetries of magnon-phonon coupling and the challenge of accurately calculating the phonon dispersion in magnetic materials, as these will be affected by the spin-lattice coupling. Also, Gennaro *et al.*[31] have combined first principle methods with atomistic spin dynamics to introduce the effect of the phonons in the fixed-lattice magnetic simulations by employing exchange parameters calculated for different relaxation of the lattice. In this work however, we directly model in a self consistent way, the dynamics of both phonons and spins and the spin-lattice coupling is treated phenomenologically similarly to[22,25–27,29], the coupling being able to efficiently exchange energy and angular momentum between the two subsystems.

SLD models have so far considered either microcanonical (NVE - constant particle number, volume and energy)[27,28] or canonical (NVT - constant particle number, volume and temperature) ensembles with two Langevin thermostats connected to both lattice and spin subsystems[23,32]. Damping due to spin-lattice interactions only within the canonical ensemble (NVT) has not yet been addressed, but is of interest in future modelling of magnetic insulators at finite temperature. Here we introduce a SLD model capable of describing both ensembles. Specifically, our model (i) takes into account the transfer of angular momentum from spin to lattice and vice-versa, (ii) works both in a microcanonical ensemble (constant energy) and in a canonical ensemble (constant temperature), (iii) al-

lows a fixed Curie temperature of the system independent of the spin-lattice coupling strength, (iv) disables uniform translational motion of the system and additional constant energy drift, which can be produced by certain spin-lattice coupling forms. Furthermore, in this work, the characteristics of the induced spin-lattice noise, the magnon-phonon induced damping and the equilibrium properties of the magnetic system has been systematically investigated.

Since many SLD models use bcc Fe due to its considerably large magneto-elastic coupling and for the necessity to include both lattice and spin degrees of freedom to capture the bcc-fcc-bcc phase transition at high temperatures[33], for the SLD model developed here we also use the parameters for this material. The aim of this work isn't however to accurately reflect the structural properties of bcc Fe, but to rather understand the effect of phonon inclusion onto the spin dynamics. Hence, Fe potentials were used because of the mere facts that they are well studied in the literature and thus we could benchmark our results with others.

The paper is organised as follows. We start by describing the computational model of Spin-Lattice Dynamics and the magnetic and mechanical energy terms used in this framework (Section II). We then explore the equilibrium properties of the system for both microcanonical and canonical simulations, proving that our model is able to efficiently transfer both energy and angular momentum between the spin and lattice degrees of freedom. In Section III we compute the equilibrium magnetisation as function of temperature for both a dynamic and static lattice and we show that the order parameter is not dependent on the details of the thermostat used. In Section IV we analyse the auto-correlation functions and spectral characteristics of magnon, phonons and the coupling term proving that the pseudo-dipolar coupling efficiently mediates the transfer of energy from spins to the lattice and vice-versa. We then calculate the temperature and coupling dependence of the induced magnon-phonon damping and we conclude that the values agree well with damping measured in magnetic insulators, where the electronic contributions to the damping can be neglected (Section V).

II. COMPUTATIONAL MODEL

In order to model the effects of both lattice and spin dynamics in magnetic materials an atomistic system is adopted with localised atomic magnetic moments at the atomic coordinates. Within this framework we solve 9N coupled equations corresponding to atomic magnetic moment (or spin), $\mathbf{S}$, atomic position, $\mathbf{r}$ and velocity, $\mathbf{v}$. The system has however 8N degrees of freedom, due to the constraint of the spin moving on an unit sphere. The model can be extended to 9N degrees of freedom by including longitudinal fluctuations[34]. We note that for the temperatures used for these simulations the contribution from longitudinal fluctuations is small, especially for bcc Fe, where the magnitude of the magnetic moments is similar between the paramagnetic and ferromagnetic state[35]. The lattice and the magnetic system can directly interact with each other via the position and spin dependent Hamiltonians. The total Hamiltonian of the system consists of a lattice $\mathcal{H}_{lat}$ and magnetic $\mathcal{H}_{mag}$ parts:

$$\mathcal{H}_{\text{tot}} = \mathcal{H}_{\text{lat}} + \mathcal{H}_{\text{mag}}. \qquad (1)$$

The lattice Hamiltonian includes the classical kinetic and pairwise inter-atomic potential energies:

$$\mathcal{H}_{\text{lat}} = \sum_i \frac{m_i \mathbf{v}_i^2}{2} + \frac{1}{2} \sum_{i,j} U(r_{ij}). \qquad (2)$$

Our model considers a harmonic potential (HP) defined as:

$$U(r_{ij}) = \begin{cases} V_0(r_{ij} - r_{ij}^0)^2/a_0^2 & r_{ij} < r_c \\ 0 & r_{ij} > r_c. \end{cases} \qquad (3)$$

where V_0 has been parametrised for BCC Fe in[27] and $a_0 = 1\text{Å}$ is a dimension scale factor. To be more specific we consider the equilibrium distances r_{ij}^0 corresponding to a symmetric BCC structure. The interaction cut-off is $r_c = 7.8\,\text{Å}$. The parameters of the potential are given in Table II. The harmonic potential has been used for simplicity, however it can lead to rather stiff lattice for a large interaction cutoff.

Another choice of the potential used in our model is an anharmonic Morse potential (MP) parameterised in[36] for BCC Fe and defined as:

$$U(r_{ij}) = \begin{cases} D[e^{-2a(r_{ij}-r_0)} - 2e^{-a(r_{ij}-r_0)}] & r_{ij} < r_c \\ 0 & r_{ij} > r_c \end{cases} \qquad (4)$$

The Morse potential approximates well the experimental phonon dispersion observed experimentally for BCC Fe[37] as shown in[38]. The phonon spectra for the choices of potential used in this work are given in Section IV. Other nonlinear choices of potential can be calculated via, for example, the embedded atom method[39,40]. One challenge of the SLD models is the the development of spin dependent many-body potentials, which are crucial for studies of the mechanical phase transitions, deformations and defects[41]. The potentials employed here are simplistic, but can approximate well the phonon spectra of bcc Fe (both for the case of the Morse potential and for a better parameterized Harmonic potential). As we will see in the next sections, the magnon properties, such as damping, are not strongly influenced by the choice of potential. Hence we have decided to remain with this simple pair-wise implementation to investigate the magnetic properties.

The spin Hamiltonian ($\mathcal{H}_{\text{mag}}$) used in our simulations consists of contributions from the exchange interaction, Zeeman energy and a spin-lattice coupling Hamiltonian, given by the pseudo-dipolar coupling term ($\mathcal{H}_{\text{c}}$), which we will describe later:

$$\mathcal{H}_{\text{mag}} = -\frac{1}{2} \sum_{i,j} J(r_{ij})(\mathbf{S}_i \cdot \mathbf{S}_j) - \sum_i \mu_i \mathbf{S}_i \cdot \mathbf{H}_{\text{app}} + \mathcal{H}_{\text{c}}, \qquad (5)$$

where μ_i is the magnetic moment of atom i, $\mathbf{S}_i$ is a unit vector describing its spin direction and $\mathbf{H}_{\text{app}}$ is an external applied magnetic field. The exchange interactions used in our simulations depend on atomic separation $J(r_{ij})$. They were calculated from first principle methods for BCC Fe by Ma *et al.*[23] and follow the dependence:

$$J(r_{ij}) = J_0 \left(1 - \frac{r_{ij}}{r_c} \right)^3 \Theta(r_c - r_{ij}), \tag{6}$$

where r_c is the cutoff and $\Theta(r_c - r_{ij})$ is the Heaviside step function, which implies no exchange coupling between spins situated at larger distance than r_c.

Several previous SLD models suffered from the fact that they did not allow angular momentum transfer between lattice and spin systems[28]. This happened for magnetisation dynamics in the absence of spin thermostat, governed by symmetric exchange only, due to total angular momentum conservation. Beaujouan *et al.*[22] has proposed a spin-pair anisotropy term in the form of a pseudo-dipolar interaction to couple the magnetisation to the lattice dynamics and to enable, for the first time, the transfer of angular momentum within the spin-lattice dynamic framework. The spatial dependence in the anisotropy term also allows the inclusion of magnetoelastic effects. Similarly, Perera *et al.*[26] proposed different local anisotropy terms to mimic the spin-orbit coupling phenomenon due to symmetry breaking of the local environment. The approach by Perera *et al.*[26] was successful in thermalising the subsystems, however, single site anisotropy spin terms with a position dependent coefficients as employed in[26] can induce an artificial collective translational motion of the sample while the system is magnetically saturated, due to the force $-\frac{\partial H_{\text{tot}}}{\partial \mathbf{r}_i}$ proportional to spin orientation. To avoid large collective motion of the atoms in the magnetic saturated state, we consider a two-site coupling term, commonly known as the pseudo-dipolar coupling, described by:

$$\mathcal{H}_c = -\sum_{i,j} f(r_{ij}) \left[(\mathbf{S}_i \cdot \hat{\mathbf{r}}_{ij})(\mathbf{S}_j \cdot \hat{\mathbf{r}}_{ij}) - \frac{1}{3}\mathbf{S}_i \cdot \mathbf{S}_j \right]. \tag{7}$$

The origin of this term still lies in the spin-orbit interaction, appearing from the dynamic crystal field that affects the electronic orbitals and spin states. This is a phenomenological term and its form comes naturally to express the coupling between two spins due to the changes in the lattice. Its biquadratic form and the exchange-like second term are necessary to avoid lattice translation in the saturated state. In reality, the coupling between phonons and magnons is material-specific and should be derived on a more strict basis. However, the goal of our paper is not to investigate magneto-elastic properties of Fe, but to construct a reasonable model of coupled spin and lattice dynamics. Several models from the literature have been tested and this simplest term was sufficient to avoid artifacts in the spin or lattice dynamics. The pseudo-dipolar coupling has been employed previously in SLD simulations, firstly by Beaujouan *et al.*[22] and followed by more recent works [25,27]. It was initially proposed by Van Vleck[42] and Akhiezer[43] as an approximation of the more complex

spin-orbit Hamiltonian and has the same structure of a dipolar interaction, however with a distance dependence that falls off rapidly, hence the name pseudo-dipolar interaction. The exchange-like term $-\frac{1}{3}\mathbf{S}_i \cdot \mathbf{S}_j$ is necessary in order to preserve the Curie temperature of the system under different coupling strengths and to ensure no net anisotropy when the atoms form a symmetric cubic lattice. For the mechanical forces, the exchange like term eliminates the anisotropic force that leads to a non-physical uniform translation of the system when the magnetic system is saturated. The magnitude of the interactions is assumed to decay as $f(\mathbf{r}_{ij}) = CJ_0(a_0/r_{ij})^4$ as presented in[27] with C taken as a constant, for simplicity measured relative to the exchange interactions and $a_0 = 1\text{Å}$ is a dimension scale factor. The constant C can be estimated from ab-initio calculations[26], approximated from magneto-elastic coefficients[27], or can be chosen to match the relaxation times and damping values, as in this work. In Ref.[26] the coupling constants of 0.1eV has been chosen, to be in the same order of magnitude as values found by first principles calculations such as Locally Self Consistent Multiple Scattering (LSMS)[44]. The above LSMS calculations with the account of thermal vibrations were reported to give the energy fluctuations in the same order of magnitude as the mean energy itself, hence the difficulty to accurately estimate the coupling energy. In Ref.[27], the coefficient C has been obtained by approximating the ratio between the pseudo-dipolar energy and exchange energy by the ratio between the magneto-elastic energy and thermal isotropic energy, $k_B T_C$.

Since the total Hamiltonian now depends on the coupled spin and lattice degrees of freedom ($\mathbf{v}_i$, $\mathbf{r}_i$, $\mathbf{S}_i$), the following equations of motion (EOM) need to be solved concurrently to obtain the dynamics of our coupled system:

$$\frac{\partial \mathbf{r}_i}{\partial t} = \mathbf{v}_i, \tag{8}$$

$$\frac{\partial \mathbf{v}_i}{\partial t} = -\eta \mathbf{v}_i + \frac{\mathbf{F}_i}{m_i}, \tag{9}$$

$$\frac{\partial \mathbf{S}_i}{\partial t} = -\gamma \mathbf{S}_i \times \mathbf{H}_i, \tag{10}$$

$$\mathbf{F}_i = -\frac{\partial \mathcal{H}_{tot}}{\partial \mathbf{r}_i} + \Gamma_i, \tag{11}$$

$$\mathbf{H}_i = -\frac{1}{\mu_S \mu_0} \frac{\partial \mathcal{H}_{tot}}{\partial \mathbf{S}_i}, \tag{12}$$

where $\mathbf{F}_i$ and $\mathbf{H}_i$ represent the effective force and field, Γ_i represents the fluctuation term (thermal force) and η represents the friction term that controls the dissipation of energy from the lattice into the external thermal reservoir. The strength of the fluctuation term can be calculated by converting the dissipation equations into a Fokker-Planck equation and then calculating the stationary solution. The thermal force has the form of a Gaussian noise:

$$\langle \Gamma_{i\alpha}(t) \rangle = 0, \tag{13}$$

$$\langle \Gamma_{i\alpha}(t)\Gamma_{j\beta}(t') \rangle = \frac{2\eta k_B T}{m_i} \delta_{\alpha\beta} \delta_{ij} \delta(t - t'). \tag{14}$$

Model	Lattice	Lattice thermostat	Spin thermostat	Intrinsic Spin damping
SLD	Dynamic	On	Off	Phonon induced
ASD	Fixed	Off	On	Electronic mainly

TABLE I. Summary comparison of the SLD model developed here against other spin dynamics models.

Quantity	Symbol	Value	Units
Exchange[23]	J_0	0.904	eV
	r_c	3.75	Å
Harmonic potential[27]	V_0	0.15	eV
	r_c	7.8	Å
Morse potential[36]	D	0.4174	eV
	a	1.3885	Å
	r_0	2.845	Å
	r_c	7.8	Å
Magnetic moment	μ_s	2.22	μ_B
Coupling constant	C	0.5	
Mass	m	55.845	u
Lattice constant	a	2.87	Å
Lattice damping	η	0.6	s^{-1}

TABLE II. Parameters used in the spin-lattice model to simulate BCC Fe.

To prove that the complete interacting many-body spin-lattice framework presented in here is in agreement with the fluctuation-dissipation theorem[45], we have followed the approach presented by Chubykalo *et al.*[46] based on the Onsager relations. Linearising the equation of motion for spins, we find that the kinetic coefficients for the spin system are zero, due to the fact that the spin and internal field are thermodynamic conjugate variables. Hence, if the noise applied to the lattice obeys the fluctuation dissipation theory, the coupled system will obey it as well, due to the precessional form of the equation of motion for the spin.

We compare the SLD model presented here with other existing model that do not take into account the lattice degrees of freedom (Atomistic Spin Dynamics - ASD). Particularly, in our case we assume a fixed lattice positions. The summary of the comparison is presented in Table I. Atomistic spin dynamics simulations (ASD)[18,20,47,48] have been widely used to study finite size effects, ultrafast magnetisation dynamics and numerous other magnetic phenomena. Here the intrinsic spin damping (the Gilbert damping - α_G) is phenomenologically included. In our case since the lattice is fixed it is assumed to come from electronic contributions. This phenomenological approach is typically used for metals, where the intrinsic damping is given by mainly electronic contributions[49–51]. Consequently, only 3N (2N degrees of freedom) equations of motion per atom describing the spin dynamics are used:

$$\frac{\partial \mathbf{S}_i}{\partial t} = -\frac{\gamma}{(1+\alpha_G^2)}\mathbf{S}_i \times (\mathbf{H}_i + \alpha_G \mathbf{S}_i \times \mathbf{H}_i) \quad (15)$$

with an additional field coming from the coupling to the fixed lattice positions. The temperature effects are introduced in spin variables by means of a Langevin thermostat. The spin thermostat is modeled by augmenting the effective fields by a thermal stochastic field ($\mathbf{H}_i = \xi_i - \partial \mathscr{H}/\partial \mathbf{S}_i$) and its properties also follow the fluctuation-dissipation theorem:

$$\langle \xi_{i\alpha}(t) \rangle = 0, \quad (16)$$

$$\langle \xi_{i\alpha}(t)\xi_{j\beta}(t') \rangle = \frac{2\alpha_G k_B T}{\gamma \mu_S}\delta_{\alpha,\beta}\delta_{ij}\delta(t-t'). \quad (17)$$

The characteristics of the above presented models are summarised in Table I.

To integrate the coupled spin and lattice equations of motion we used a Suzuki-Trotter decomposition (STD) method[52] known for its numerical accuracy and stability. The scheme can integrate non-commuting operators, such as is the case of

spin-lattice models and conserves the energy and space-phase volume. The conservation of energy is necessary when dealing with microcanonical simulations. Considering the generalized coordinate $\mathbf{X} = \{\mathbf{r}, \mathbf{v}, \mathbf{S}\}$ the equations of motion can be re-written using the Liouville operators:

$$\frac{\partial \mathbf{X}}{\partial t} = \hat{L}\mathbf{X(t)} = (\hat{L}_r + \hat{L}_v + \hat{L}_S)\mathbf{X}(t). \quad (18)$$

The solution for the Liouville equation is $\mathbf{X}(t + \Delta t) = e^{L\Delta t}\mathbf{X}(t)$. Hence, following the form of this solution and applying a Suzuki-Trotter decomposition as in Tsai's work[53,54], we can write the solution as:

$$\mathbf{X}(t+\Delta t) = e^{\hat{L}_s \frac{\Delta t}{2}}e^{\hat{L}_v \frac{\Delta t}{2}}e^{\hat{L}_r \Delta t}e^{\hat{L}_v \frac{\Delta t}{2}}e^{\hat{L}_s \frac{\Delta t}{2}}\mathbf{X}(t) + O(\Delta t^3), \quad (19)$$

where L_s, L_v, L_r are the Liouville operators for the spin, velocity and position. This update can be abbreviated as (s,v,r,v,s) update. The velocity and position are updated using a first order update, however the spin needs to be updated using a Cayley transform[55,56], due to the fact that the norm of each individual spin needs to be conserved. Thus we have

$$e^{\hat{L}_v \Delta t}\mathbf{v}_i = \mathbf{v}_i + \frac{\Delta t}{m_i}\mathbf{F}_i, \quad (20)$$

$$e^{\hat{L}_r \Delta t}\mathbf{r}_i = \mathbf{r}_i + \Delta t \mathbf{v}_i, \quad (21)$$

$$e^{\hat{L}_s \Delta t}\mathbf{S}_i = \frac{\mathbf{S}_i + \Delta t \mathbf{H}_i \times \mathbf{S}_i + \frac{\Delta t^2}{2}\left[(\mathbf{H}_i \cdot \mathbf{S}_i)\mathbf{H}_i - \frac{1}{2}\mathbf{H}_i^2 \mathbf{S}_i\right]}{1 + \frac{1}{4}\Delta t^2 \mathbf{H}_i^2}. \quad (22)$$

The spin equations of motions depend directly on the neighbouring spin orientations (through the effective field) hence individual spins do not commute with each other. We need to further decompose the spin system $\hat{L}_s = \sum_i \hat{L}_{s_i}$. The following decomposition will be applied for the spin system:

$$e^{\hat{L}_s(\Delta t/2)} = e^{\hat{L}_{s_1}(\Delta t/4)}...e^{\hat{L}_{s_N}(\Delta t/2)}...e^{\hat{L}_{s_1}(\Delta t/4)} + O(\Delta t^3) \quad (23)$$

Tests of the accuracy of the integration have been performed by checking the conservation of energy within the microcanonical ensemble. To ensure that the spin and lattice

sub-systems have reached equilibrium, we calculate both the lattice temperature (from the Equipartition Theorem) and spin temperature[57]. These are defined as:

$$T_L = \frac{2}{3Nk_B} \sum_i \frac{\mathbf{p}_i^2}{2m}, \quad T_S = \frac{\sum_i (\mathbf{S}_i \times \mathbf{H}_i)^2}{2k_B \sum_i \mathbf{S}_i \cdot \mathbf{H}_i}. \quad (24)$$

III. SPIN-LATTICE THERMALISATION

As an initial test of our model we look at the thermalisation process within micro-canonical (NVE) and canonical (NVT) simulations for a periodic BCC Fe system of $10 \times 10 \times 10$ unit cells. No thermostat is applied directly to the spin system and its thermalisation occurs via transfer of energy and angular momentum from the lattice, i.e. via the magnon-phonon interaction. In the case of the NVE simulations, the energy is deposited into the lattice by randomly displacing the atoms from an equilibrium BCC structure positions within a 0.01 Å radius sphere and by initialising their velocities with a Boltzmann distribution at $T = 1200$ K. The spin system is initialised on the z direction, corresponding to a spin temperature $T_S = 0K$. In the case of NVT simulations, the lattice is connected to a thermostat at a temperature of $T = 800$ K. The parameters used in the simulations are presented in Table II.

Fig. 1 shows the thermalisation process for the two types of simulation. In both cases the spin system has an initial temperature of $T_S = 0$ K corresponding to a saturated state in the z direction. For the NVE simulations, the two subsystems are seen to equilibrate at a temperature of $T = 445$ K, this temperature being dependent on the energy initially deposited into the system. In the NVT simulations, the lattice is thermalised at $T = 800$ K followed by the relaxation of the spin towards the same temperature. In both cases we observe that the relaxation of the spin system happens under 1ns, the relaxation timescale being dependent on the initial temperature of the sub-systems. Since the spin sub-system is initialised at $T_S = 0$K, the relaxation is slower, and overcomes the typical 100ps values observed typically for spin-lattice relaxation. The corresponding change in the magnetisation is emphasized by the green lines in Fig. 1 showing a transfer of angular momentum between the spin and lattice degrees of freedom. Fig. 2 shows the variation of the total energy E_T, the lattice energy E_L and spin energy E_S for both NVE and NVT simulations. The total energy is conserved for the NVE simulation and it is distributed between the lattice and spin degrees of freedom. For the NVT simulations, the total energy presents thermal fluctuations around a constant value, after an initial relaxation regime. We have also investigated the energy variation as function of the integration time-step and concluded that an integration time-step of $t_s = 0.5fs$ is sufficient to conserve the energy within the numerical precision of the simulations whilst keeping low computational cost.

To gain a better understanding of properties at thermal equilibrium within the Spin-Lattice Dynamics model, we have investigated the temperature dependence of the magnetic order parameter in different frameworks that either enable or dis-
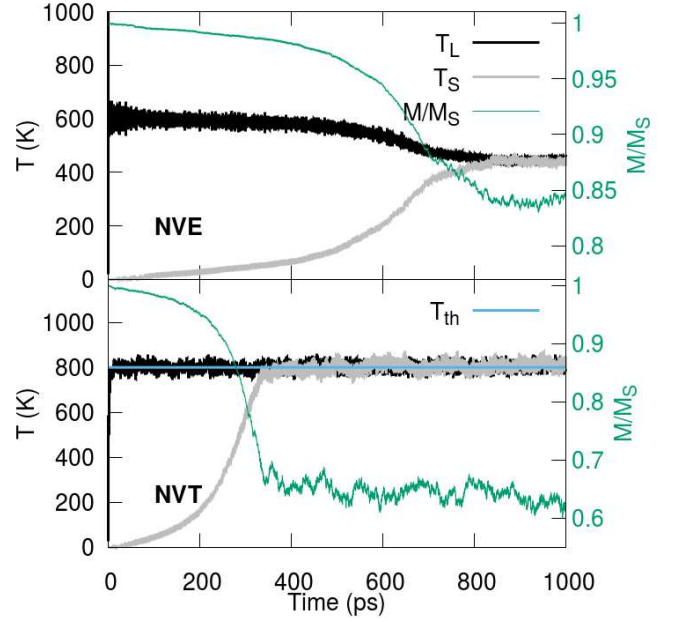

FIG. 1. NVE (top) and NVT (bottom) simulations for a $10 \times 10 \times 10$ unit cell BCC Fe system. The spin system is initialised at $T_S = 0$K corresponding to a saturated magnetic state in the z direction, while the lattice velocities are initialised by a Boltzmann distribution at $T_L = 1200$ K (for NVE) and $T_L = 600$ K (for NVT). In both cases we obtain equilibration of the two subsystems under 1ns.

able lattice dynamics, specifically: SLD or ASD. Tab. I illustrates the differences between the models. Since reaching joint thermal equilibrium depends strongly on the randomness already present in the magnetic system this process is accelerated by starting with a reduced magnetisation of $M/M_S = 0.9$ for $T > 300$ K.

Fig. 3 shows the comparison of the equilibrium magnetisation using either the harmonic potential (HP), Morse potential (MP) or fixed lattice (ASD) simulations. The magnetisation is calculated by averaging for 200 ps after an initial equilibration for 800 ps (for SLD type simulations) or 100 ps (for ASD) simulations. We observe that even without a spin thermostat (in SLD model) the magnetisation reaches equilibrium via the thermal fluctuations of the lattice, proving that both energy and angular momentum can be successfully transferred between the two sub-systems. Additionally, both the SLD and ASD methods give the same equilibrium magnetisation over the temperature range considered. This confirms that the equilibrium quantities are independent of the details of the thermostat used, in agreement with the fact that both SLD and ASD models obey the fluctuation-dissipation theorem.

In principle, since the strength of the exchange interaction depends on the relative separation between the atoms, any thermal expansion of the lattice could potentially modify the Curie temperature. However, as highlighted in the inset of Fig. 3, the same Curie temperature is observed in each model. We attribute this to fact that the thermal lattice expansion is small in the temperature range considered due to two reasons:
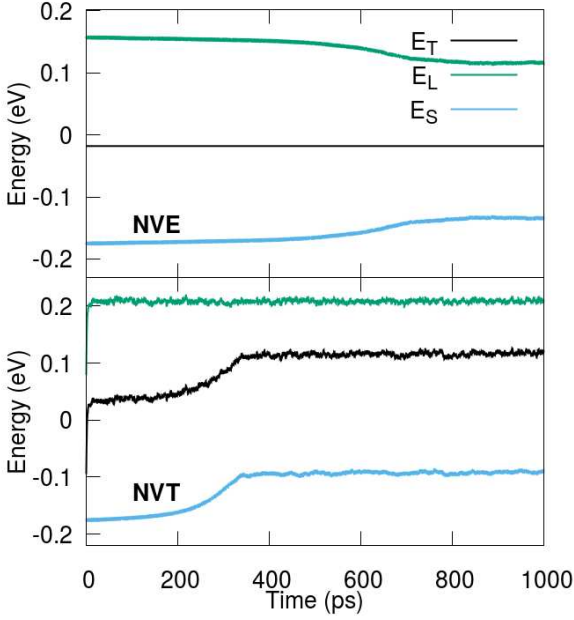
FIG. 2. Energies for NVE (top) and NVT (bottom) simulations for a $10 \times 10 \times 10$ unit cell BCC Fe system corresponding to the simulations presented in Fig. 1.
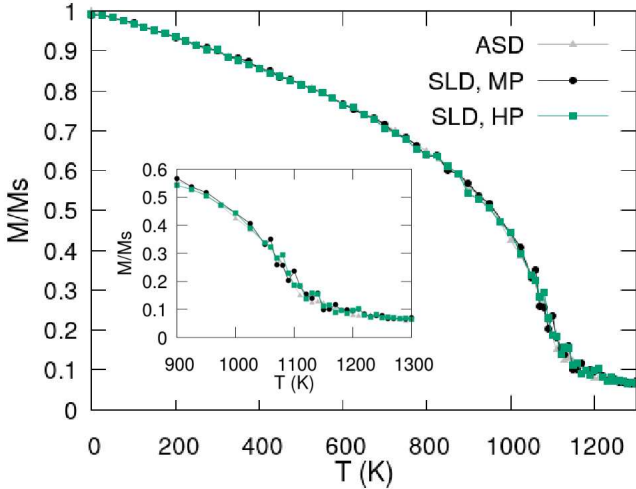

FIG. 3. Magnetisation versus temperature curves for the SLD model (with different choices of lattice potential: MP-Morse Potential, HP-Harmonic Potential) and fixed lattice ASD model. The inset zooms around the ferromagnetic to paramagnetic phase transition temperature.

i) the Curie temperature of the system is well below the melting point of Fe ($\approx 1800\,\mathrm{K}$) and ii) we model a bulk, constant-volume system with periodic boundary conditions that does not present strong lattice displacements due to surfaces. We note that Evans *et al.*[58] found a reduction of T_C in nanoparticles due to an expansion of atomic separations at the surface that consequently reduces the exchange interactions. For systems with periodic boundary conditions we anticipate fluctua-

tions in the exchange parameter due to changes in interatomic spacings to be relatively small. Our calculations of effective exchange constant for a dynamic lattice showed a variation of about 1% with respect to the static lattice, difference that it is not reflected in the equilibrium magnetisation curves. By removing the periodicity of the system, different Curie temperatures can be observed between the static and dynamic lattice case, due to the surface effects that induce a variation of the effective exchange constant in the order of 10%. Santos *et al.*[59] have performed a systematic comparison of the finite size effects of the magnetisation of static and dynamic lattice calculation and their results showed differences between the two even in the case of periodic systems. This suggests that the individual parameterisation of the exchange and inter-atomic potential can largely influence the behaviour of the equilibrium magnetisation. Although, for the parametrisation used in this work we show that the equilibrium properties are not dependent on the details of the thermostat or the potential, the magnetisation dynamics could be strongly influenced by these choices.

The strength of the pseudo-dipolar coupling parameters C determines the timescale of the thermalisation process. Its value can be parametrised from magneto-elastic simulations via calculations of the anisotropy energy as a function of strain. The magneto-elastic Hamiltonian can be written for a continuous magnetisation $\mathbf{M}$ and elastic strain tensor $\mathbf{e}$ as[60,61]:

$$\mathscr{H}_{\mathrm{m-e}} = \frac{B_1}{M_S^2}\sum_i M_i^2 e_{ii} + \frac{B_2}{M_s^2}\sum_i M_i M_j e_{ij} \qquad (25)$$

where constants B_1, B_2 can be measured experimentally[62]. The pseudo-dipolar term acts as a local anisotropy, however, for a lattice distorted randomly, this effective anisotropy is averaged out to zero. At the same time under external strain effects, an effective anisotropy will arise due to the pseudo-dipolar coupling which is the origin of the magneto-elastic effects. To calculate the induced magnetic anisotropy energy (MAE), the BCC lattice is strained along the z direction whilst fixed in the xy plane. The sample is then uniformly rotated and the energy barrier is evaluated from the angular dependence of the energy. Fig. 4 shows MAE for different strain values and coupling strengths, with the magneto-elastic energy densities constants B_1 obtained from the linear fit. The values of the obtained constants B_1 are larger than the typical values reported for BCC Fe $B_1 = -3.43\,\mathrm{MJ\,m^{-3}} = -2.14 \times 10^{-5}$ eV A^{-3}[62] measured at $T = 300$ K which is similar to the B_1 value obtained for small coupling strengths $C = 0.018$. However a larger coupling $C = 0.5$ is necessary in order to obtain damping parameters comparable to the ones known for magnetic insulators where the main contribution comes from magnon-phonon scattering. In reality, in BCC Fe there is an important contribution to the effective damping from electronic sources, which if considered, can lead to the smaller coupling strengths, consistent in magnitude with experimental magneto-elastic parameters. Indeed, as we will show later, our finding suggests that phonon damping is a very small contribution in metallic systems such as BCC Fe .
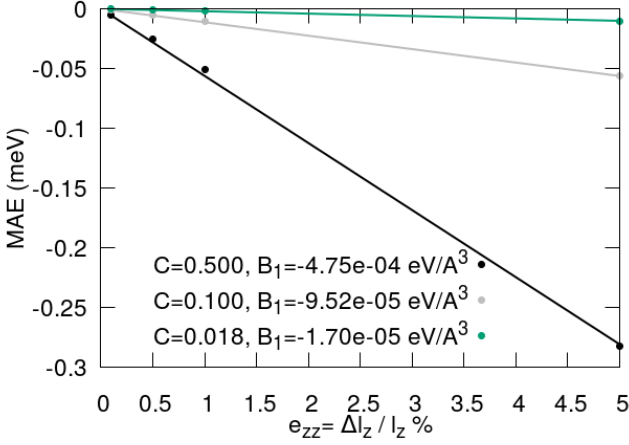
FIG. 4. Magnetic anisotropy energy as function of strain for different coupling strengths for T=0K.

IV. DYNAMIC PROPERTIES AT THERMAL EQUILIBRIUM

Section III showed that the equilibrium magnetisation does not depend on the details of the thermostat used and a successful transfer of both energy and angular momentum is achieved between the spin and lattice sub-systems by the introduction of a pseudo-dipolar coupling term. In this section, we investigate the properties of the magnons, phonons and the coupling term that equilibrates the spin and phonon systems in the absence of a phenomenological spin damping. Two types of simulations are presented here: i) magnon and phonon spectra calculated along the high symmetry path of a BCC lattice and ii) averaged temporal Fourier transform (FT) of individual atoms datasets (spin, velocity, pseudo-dipolar coupling field). The phonon - Fig. 5 and magnon - Fig. 6 spectra are calculated by initially equilibrating the system for 10 ps with a spin thermostat with $\alpha_G = 0.01$ and a coupling of $C = 0.5$, followed by 10 ps of equilibration in the absence of a spin thermostat. For the method i) the correlations are computed for a runtime of 20 ps after the above thermalisation stage. For each point in k-space, the first three maxima of the auto-correlation function are plotted for better visualisation. The auto-correlation function is projected onto the frequency space and the average intensity is plotted for different frequencies. The phonon spectra are calculated from the velocity auto-correlation function defined in Fourier space as[38,63]:

$$A^p(k,\omega) = \int_0^{t_f} \langle v_k^p(t)v_k^p(t-t')\rangle e^{-i\omega t}dt \quad (26)$$

where $p = x,y,z$, t_f is the total time and $v_k^p(t)$ is the spatial Fourier Transform calculated numerically as a discrete Fourier Transform:

$$v_k^p(t) = \sum_i v_i^p e^{-i\mathbf{k}\cdot\mathbf{r_i}} \quad (27)$$

The same approach is applied for the magnon spectra, using the dynamical spin structure factor, which is given by

the space-time Fourier transform of the spin-spin correlation function defined as $C^{mn}(r-r',t-t') = < S^m(r,t)S^n(r',t') >$, with m,n given by the x,y,z components[64]:

$$S^{mn}(\mathbf{k},\omega) = \sum_{r,r'} e^{i\mathbf{k}\cdot(\mathbf{r}-\mathbf{r'})} \int_0^{t_f} C^{mn}(r-r',t-t')e^{-i\omega t}dt \quad (28)$$

The second method (ii)) to investigate the properties of the system involves calculating temporal Fourier transform of individual atoms datasets, and averaging the Fourier response over 1000 atoms of the system. This response represents an integrated response over the k-space. Hence, the projection of intensities on the frequency space presented by method i) has similar features as the spectra presented by method ii). For the results presented in Fig. 7, a system of $10 \times 10 \times 10$ BCC unit cells has been chosen. The system has been equilibrated for a total time of 20 ps with the method presented in i) and the Fast Fourier transform (FFT) is computed for the following 100 ps.

Fig. 5 shows the phonon spectra for a SLD simulations at $T = 300K$, $C = 0.5$ for the Morse Potential - Fig. 5(a) and the Harmonic Potential - Fig. 5(b) calculated for the high symmetry path of a BCC system with respect to both energy and frequency units. The interaction cutoff for both Morse and Harmonic potential is $r_c = 7.8\,\text{Å}$. The Morse phonon spectrum agrees well with the spectrum observed experimentally[37] and with the results from[38]. The projection of the spectra onto the frequency domain shows a peak close to 10.5 THz, due to the overlap of multiple phonon branches at that frequency and consequently a large spectral density with many k-points excited at this frequency. Moving now to the harmonic potential, parameterised as in Ref. 27, we first note that we observe that some of the phonon branches overlap - Fig.5b). Secondly, the projection of intensity onto the frequency domain shows a large peak at 8.6THz, due to a flat region in the phonon spectra producing even larger number of k-points in the spectrum which contribute to this frequency. Finally, the large cutoff makes the Harmonic potential stiffer as all interactions are defined by the same energy, V_0, and their equilibrium positions corresponding to a BCC structure. This is not the case for the Morse potential which depends exponentially on the difference between the inter-atomic distance and a constant equilibrium distance, r_0. For a long interaction range, the harmonic approximation will result in a more stiff lattice than the Morse parameterisation.

In principle, the harmonic potential with a decreased interaction cutoff and an increased strength could better reproduce the full phonon spectra symmetry for BCC Fe. However, in this work we preferred to use the parameterisation existing in literature[27] and a large interaction cutoff for stability purposes. Although the full symmetry of the BCC Fe phonon spectra is not reproduced by this harmonic potential, the phonon energies/frequencies are comparable to the values obtained with the Morse potential. Nevertheless, we observed the same equilibrium magnetisation and damping (discussed later) for both potentials, hence the simple harmonic potential represents a suitable approximation, that has the advantage of being more computationally efficient.
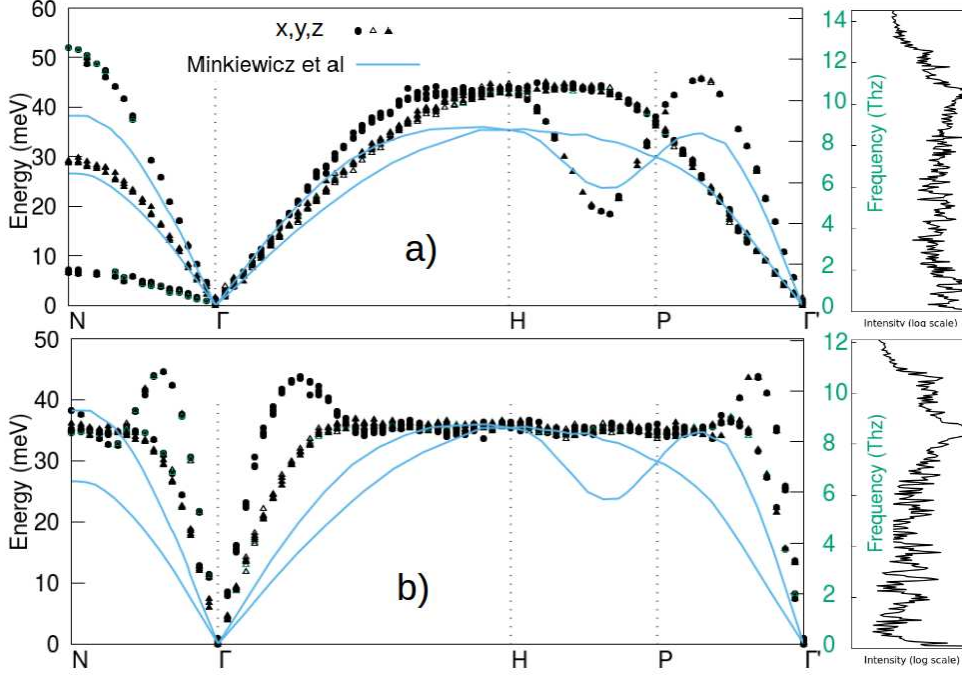
FIG. 5. Phonon spectra calculated for a $32 \times 32 \times 32$ unit cell system at $T = 300$K, $C = 0.5$ for a) Morse potential, b)Harmonic potential. The spectra are calculated via method i). Right figure includes the projection of the intensity of the spectra onto the frequency domain. Solid lines are the experimental data of Minkiewicz et $al.$[37]. For the Minkiewicz et $al.$ data there is only 1 datapoint for the N-Γ path for the second transverse mode which does not show up on the line plots.

Fig. 6 shows the magnon spectrum obtained within the SLD framework using the Morse potential together with its projection onto the frequency domain. The results agree very well with previous calculations of magnon spectra[28,65] and with the experimental magnon dispersion measured by Loong et $al.$[66]. For the comparison against experiments, we have used the analytical dispersion equation $Dq^2(1 - \beta q^2)$, where the parameters $D = 307$meV, $\beta = 0.32$meVÅ^2 have been extracted from experimental measurements. The inset of Fig. 6 shows the behavior of the dispersion for low-q values. For the harmonic potential the magnon spectrum is found to be identical to that for the Morse potential with only very small changes regarding the projection of intensity onto the frequency domain. This is in line with our discussion in the previous section where the choice of inter-atomic potential had little effect on the Curie temperature, which is closely linked to the magnonic properties. As the harmonic potential is more computationally efficient than the Morse, we next analyse the properties of the system for a $10 \times 10 \times 10$ unit cells system at $T = 300$K with the harmonic potential.

The power spectral density (auto-correlation in Fourier space) of the magnon, phonons and coupling field at 300 K is shown in Fig. 7 computed using method ii detailed previously. The amplitude of the FFT spectra of velocities and coupling field has been scaled by 0.12 and 0.05 respectively to allow for an easier comparison between these quantities. As shown in Fig. 7.a) the coupling term presents both magnon and phonon characteristics; demonstrating an efficient coupling of the two sub-systems. The large peak observed at

a frequency of 8.6 THz appears as a consequence of the flat phonon spectrum for a Harmonic potential, as observed in the spectrum and its projection onto the frequency domain in Fig. 5.b). Additionally, Fig. 7.a) can give us an insight into the induced spin noise within the SLD framework. The background of the FFT of the coupling field is flat for the frequencies plotted here, showing that the noise that acts on the spin is uncorrelated. The inset shows a larger frequency domain where it is clear that there are no phonon modes for these frequencies, and only thermal noise decaying with frequency is visible. At the same time an excitation of spin modes are visible for frequencies up to ca .100 THz.

The characteristics of the coupling field with respect to the coupling strength for a dynamic (SLD) and fixed lattice simulations (ASD) are presented in Fig. 7(b). The only difference between the ASD and SLD simulations is given by the presence of phonons (lattice fluctuations) in the latter. Since the large peak at 8.6 THz is due to the lattice vibrations, it is not present in the ASD simulations. The smaller peaks are present in both models since they are proper magnonic modes. With increasing coupling the width of the peaks increases suggesting that the magnon-phonon damping has increased. Moving towards the larger frequency regimes, Fig. 7.b) - (inset), we observe that large coupling gives rise to a plateau in the spectra at around 150 THz, which is present as well for the fixed-lattice simulations (ASD). The plateau arises from a weak antiferromagnetic exchange that appears at large distances due to the competition between the ferromagnetic exchange and the antiferromagnetic exchange-like term in the pseudo-dipolar
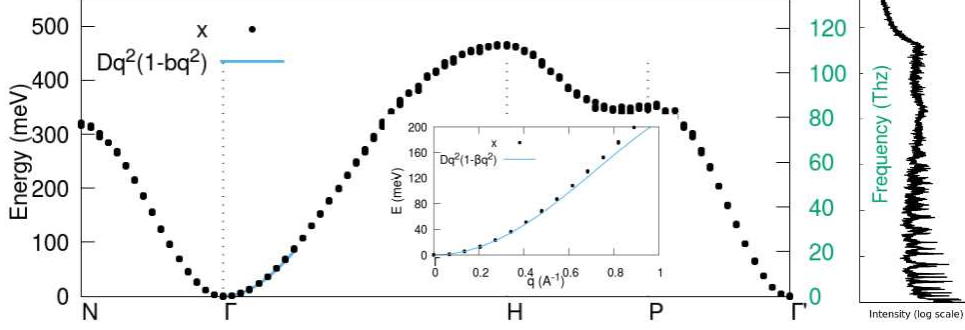
FIG. 6. Magnon spectrum (x component) calculated for a $32 \times 32 \times 32$ unit cell system at $T = 300$K, $C = 0.5$ for a Morse potential. The spectrum is calculated via method i). The blue line is given by the dispersion equation $Dq^2(1 - \beta q^2)$, where the parameters $D = 307$meV, $\beta = 0.32$meV$\mathring{A}^2$ have been extracted from experimental measurements by Loong $et\ al.$[66]. The inset shows the behavior of the dispersion for low-q values.

Right figure includes the projection of the intensity of the spectrum onto the frequency domain.
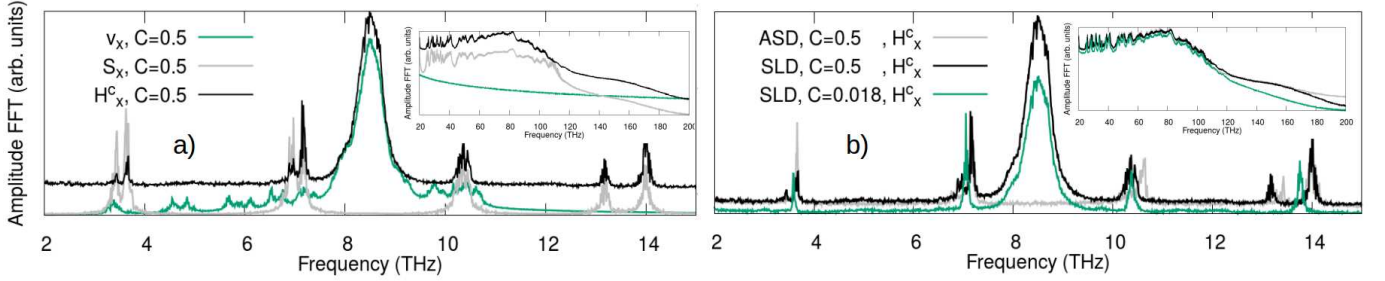

FIG. 7. The power spectral density of the auto-correlation function in the frequency domain for magnons, phonons and coupling field for a SLD simulations with a Harmonic lattice, calculated by method ii). Panel a) shows the power density of the auto-correlation function of the x component of the velocity v_x, spin S_x and coupling field H_x^c. Panel b) presents the power density of the auto-correlation function for the x component of the coupling field for either static (ASD) or dynamic (SLD) lattice. The insets show the high-frequency spectra. For Panel a) the velocity and the coupling field have been multiplied by a factor of 0.12 and 0.05 respectively for easier graphical comparison.

coupling.

We have also analysed the characteristics of the magnon and phonon spectra for different temperatures- Fig. 8. With increasing temperature, the peaks corresponding to magnons shift to smaller frequencies. This is a typical situation known as a softening of low-frequency magnon modes due to the influence of thermal population, see e.g.[67] - Panel a). The same effect can be observed by calculating the magnon spectra via method i for various temperatures. In Panel b), the peak corresponding to phonons remains almost at the same frequency of about 8.6 THz, as the phonon spectra is not largely affected by temperatures up to $T = 600$K. The increase of the effective damping (larger broadening) of each magnon mode with temperature is clearly observed.

V. MACROSOPIC MAGNETISATION DAMPING

In this section we evaluate the macroscopic damping parameter experienced by magnetisation due to the magnon-phonon excitations for a periodic BCC system using our SLD model. This method for calculating the damping has been presented in[68–70]. The system is first thermalised at a non-zero temperature in an external field of $B_{ext} = 50$T applied in the z direction, then the magnetisation is rotated coherently through an angle of $30°$. The system then relaxes back to equilibrium allowing the relaxation time to be extracted. The averaged z component of magnetisation is then fitted to the function $m_z(t) = \tanh(\alpha \gamma B_{ext}(t + t_0)/(1 + \alpha^2))$ where α represents the macrosopic (LLG-like) damping, γ the gyromagnetic ratio and t_0 a constant related to the initial conditions. The model system consists of $10 \times 10 \times 10$ unit cells and the damping value obtained from fitting of $m_z(t)$ is averaged over 10 different simulations.

Fig. 9 shows the dependence of the average damping parameter together with the values obtained from individual simulations for different temperatures and coupling strengths for two choices of mechanical potential. In our model, the spin system is thermalised by the phonon thermostat, hence no electronic damping is present. With increasing coupling, the energy and angular momentum transfer is more efficient, hence the damping is enhanced. Since the observed value of induced damping is small, calculating the damping at higher temperature is challenging due to the strong thermal fluctua-
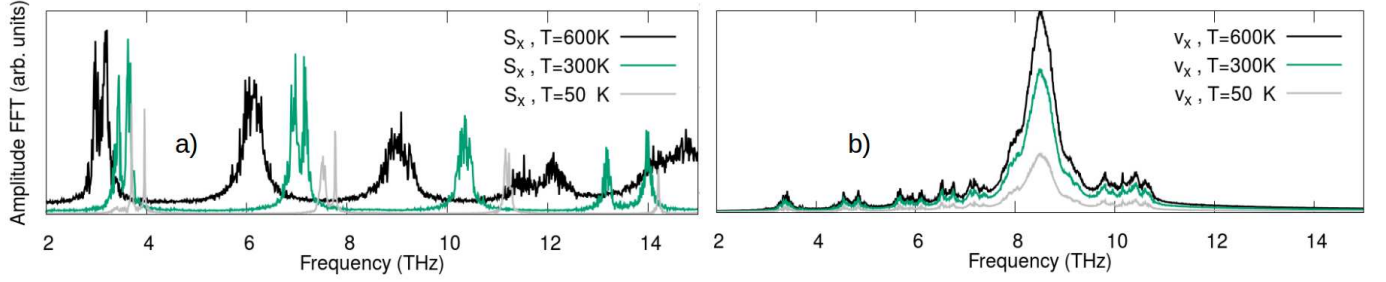
FIG. 8. The power spectral density of the auto-correlation function in the frequency domain for magnons - Panel a) and phonons - Panel b) for a SLD simulations with a Harmonic lattice, calculated by method *ii)*, for three distinct temperatures and a coupling constant of $C = 0.5$.
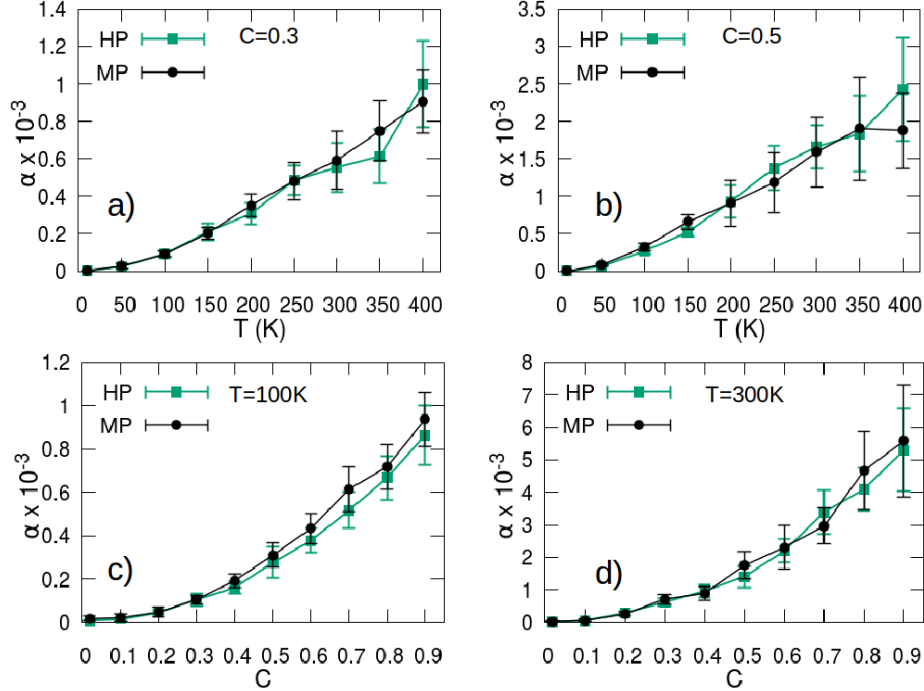

FIG. 9. Damping parameter extracted from fitting the z component of the magnetisation for two different choices of potential: HP- Harmonic Potential (green open squares) and MP-Morse Potential (black open circles) as function of temperature Fig. a), b) and as function of the coupling strength Fig. c), d); Fig a) and b) are calculated for a constant coupling strength of $C = 0.3$, $C = 0.5$ respectively. Fig c) and d) are calculated for temperatures of $T = 100K$, $T = 300K$ respectively. The black and green lines represents the average damping parameter obtained from the simulations using the Morse and the Harmonic Potentials, respectively.

tions that affect the accuracy of the results. Despite the low temperatures simulated here, the obtained damping values (at $T = 50K$, $\alpha = 4.9 \times 10^{-5}$) are of the same order as reported for magnetic insulators such as YIG (1×10^{-4} to 1×10^{-6}[71,72]) as well as in different SLD simulations (3×10^{-5},[27]). Generally, the induced damping value depends on the phonon characteristics and the coupling term, that allows transfer of both energy and angular momentum between the two subsystems.

Fig. 9(a) and (b) compare the calculated damping for the Morse and Harmonic potential for two values of the coupling strength. We observe that the values are not greatly affected by the choice of potential. This arises due to the fact that only the spin modes around Γ point are excited and for this low k-

vectors modes the inter-atomic distances between neighbouring atoms do not vary significantly. The extracted damping parameter as a function of coupling strength for 100 K and 300 K is presented in Fig. 9(c) and (d) respectively. The functional form of the variation is quadratic, in accordance with the form of the coupling term. Measurements of damping in magnetic insulators, such as YIG, show a linear increase in the damping with temperature,[72] which agrees with the relaxation rates calculated by Kasuya and LeCraw[73] and the relaxation rates calculated in the NVE SLD simulations in Ref. 27. However, Kasuya and LeCraw suggest that the relaxation rate can vary as T^n, where $n = 1 - 2$ with $n = 2$ corresponding to larger temperature regimes. Nevertheless, the difference between
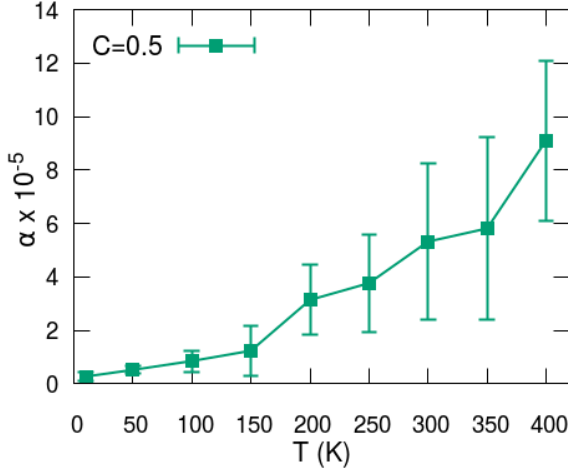
FIG. 10. Temperature variation of the damping parameter for Néel-like on-site coupling, $H_c = -\sum_{i,j} f(r_{ij})((\mathbf{S}_i \cdot \hat{\mathbf{r}}_{ij})^2 - \frac{1}{3}\mathbf{S}_i^2)$. The values are extracted from $m_z(t)$ fittings for 10 realisations;

the quadratic temperature variation of the damping observed in our simulations and the linear one observed in experiments for YIG can be attributed to the difference in complexity between the BCC Fe model and YIG. The difference between the trends may as well suggest that the spin-orbit coupling in YIG could be described better by a linear phenomenological coupling term, such as the one used in Refs. 26 and 29, but we note that such forms can lead to a uniform force in the direction of the magnetisation and so might need further adaptation before being suitable. To test an alternate form of the coupling we have replaced the pseudo-dipolar coupling to an on-site form, specifically $\mathscr{H}_c = -\sum_{i,j} f(r_{ij})((\mathbf{S}_i \cdot \hat{\mathbf{r}}_{ij})^2 - \frac{1}{3}\mathbf{S}_i^2)$ i.e a Néel-like anisotropy term. This is a test to understand the effect of the coupling term on the damping. The form of this coupling term leads to much smaller damping as shown in Fig. 10 ($T = 300$ K, $\alpha = 5.32 \times 10^{-5}$, averaged over 10 realisations) making it difficult to accurately calculate the temperature dependence of the damping, especially for large temperatures. The magnon-phonon damping can clearly have complex behavior depending on the properties of the system, especially the coupling term, hence no universal behaviour of damping as function of temperature can be deduced for spin-lattice models.

Neglecting the lattice contribution, the temperature dependence of the macrosopic damping can be mapped onto the Landau-Lifshitz-Bloch formalism (LLB)[68] and theory[17] and ASD simulations[74] have shown it to vary inversely with the equilibrium magnetisation. The LLB theory shows that the macrosopic damping is enhanced for large temperatures due to thermal spin fluctuations. Using the equilibrium magnetisation it is possible to approximate the variation of damping with temperature produced due to thermal fluctuations within the LLB model. From 100K to 400K the damping calculated via the LLB model increases within the order of 10^{-5}, which is considerably smaller than the results obtained via the SLD model. This shows that within the SLD model the temperature increase of the damping parameter is predominantly due to

magnon-phonon interaction, and not due to thermal magnon scattering, as this process is predominant at larger temperatures.

VI. CONCLUSIONS AND OUTLOOK

To summarise, we have developed a SLD model that is able to transfer energy and angular momentum efficiently from the spin to lattice sub-systems and vice-versa via a pseudo-dipolar coupling term. Our approached takes the best features from several previously suggested models and generalize them which allows modelling in both canonical and microcanonical ensembles. With only the lattice coupled to a thermal reservoir and not the spin system, we reproduce the temperature dependence of the equilibrium magnetisation, which agrees with the fact that the spin-lattice model obeys the fluctuation-dissipation theorem. We are able to study the dynamic properties such as phonon and spin spectrum and macrosopic damping, showing that the magnetic damping is not greatly influenced by the choice of potential, however it is influenced by the form of the coupling term. This enables the possibility of tailoring the form of the coupling term so it can reproduce experimental dependencies of damping for different materials. We also find that the experimental magneto-elastic coupling B_1 can be reproduced by selecting the correct pseudo-dipolar coupling strength. In future, the addition of quantum statistics for Spin Lattice Dynamics models[75,76] may also yield better agreement with experimental data.

The SLD model developed here opens the possibility of the investigation of ultrafast dynamics experiments and theoretically studies of the mechanism through which angular momentum can be transferred from spin to the lattice at ultrafast timescales. As we have demonstrated that the model works well in the absence of an phenomenological Gilbert damping, which consists mainly of electronic contributions, the SLD model can be employed to study magnetic insulators, such as YIG, where the principal contribution to damping is via magnon-phonon interactions. Future application of this model includes controlling the magnetisation via THz phonons[7] which can lead to non-dissipative switching of the magnetisation[11,12]. With the increased volume of data stored, field-free, heat-free switching of magnetic bits could represent the future of energy efficient recording media applications. Another possible application is more advanced modeling of the ultrafast Einstein-de-Haas effect[2] or phonon-spin transport[77].

VII. ACKNOWLEDGEMENTS

[1] E. Beaurepaire, J.-C. Merle, A. Daunois, and J.-Y. Bigot, "Ultra-fast spin dynamics in ferromagnetic nickel," Phys. Rev. Lett. **76**, 4250–4253 (1996).

[2] C. Dornes, Y. Acremann, M. Savoini, M. Kubli, M. J. Neugebauer, E. Abreu, L. Huber, G. Lantz, C. A.F. Vaz, H. Lemke, E. M. Bothschafter, M. Porer, V. Esposito, L. Rettig, M. Buzzi, M. Alberca, Y. W. Windsor, P. Beaud, U. Staub, Diling Zhu, Sanghoon Song, J. M. Glownia, and S. L. Johnson, "The ultrafast Einstein–de Haas effect," Nature **565**, 209–212 (2019).

[3] Jakob Walowski and Markus Münzenberg, "Perspective: Ultra-fast magnetism and THz spintronics," J. Appl. Phys. **120** (2016).

[4] I. Radu, C. Stamm, A. Eschenlohr, F. Radu, R. Abrudan, K. Vahaplar, T. Kachel, N. Pontius, R. Mitzner, K. Holldack, A. Föhlisch, T. A. Ostler, J. H. Mentink, R. F.L. Evans, R. W. Chantrell, A. Tsukamoto, A. Itoh, A. Kirilyuk, A. V. Kimel, and Th Rasing, "Ultrafast and Distinct Spin Dynamics in Magnetic Alloys," Spin **5**, 1–10 (2015).

[5] Martin Hennecke, Ilie Radu, Radu Abrudan, Torsten Kachel, Karsten Holldack, Rolf Mitzner, Arata Tsukamoto, and Stefan Eisebitt, "Angular Momentum Flow during Ultrafast Demagnetization of a Ferrimagnet," Phys. Rev. Lett. **122**, 157202 (2019).

[6] Sebastian F. Maehrlein, Ilie Radu, Pablo Maldonado, Alexander Paarmann, Michael Gensch, Alexandra M. Kalashnikova, Roman V. Pisarev, Martin Wolf, Peter M. Oppeneer, Joseph Barker, and Tobias Kampfrath, "Dissecting spin-phonon equilibration in ferrimagnetic insulators by ultrafast lattice excitation," Sci. Adv. **4** (2018).

[7] A. Melnikov, I. Radu, U. Bovensiepen, O. Krupin, K. Starke, E. Matthias, and M. Wolf, "Coherent optical phonons and parametrically coupled magnons induced by femtosecond laser excitation of the gd(0001) surface," Phys. Rev. Lett. **91**, 227403 (2003).

[8] Ji-Wan Kim, Mircea Vomir, and Jean-Yves Bigot, "Controlling the spins angular momentum in ferromagnets with sequences of picosecond acoustic pulses," Sci. Rep. **5**, 8511 (2015).

[9] Ji-Wan Kim, Mircea Vomir, and Jean-Yves Bigot, "Ultrafast magnetoacoustics in nickel films," Phys. Rev. Lett. **109**, 166601 (2012).

[10] A. V. Scherbakov, A. S. Salasyuk, A. V. Akimov, X. Liu, M. Bombeck, C. Bruggemann, D. R. Yakovlev, V. F. Sapega, J. K. Furdyna, and M. Bayer, "Coherent magnetization precession in ferromagnetic (ga,mn)as induced by picosecond acoustic pulses," Phys. Rev. Lett. **105**, 117204 (2010).

[11] Vladimir S. Vlasov, Alexey M. Lomonosov, Anton V. Golov, Leonid N. Kotov, Valentin Besse, Alexandr Alekhin, Dmitry A. Kuzmin, Igor V. Bychkov, and Vasily V. Temnov, "Magnetization switching in bistable nanomagnets by picosecond pulses of surface acoustic waves," Phys. Rev. B **101**, 024425 (2020).

[12] Oleksandr Kovalenko, Thomas Pezeril, and Vasily V. Temnov, "New concept for magnetization switching by ultrafast acoustic pulses," Phys. Rev. Lett. **110**, 266602 (2013).

[13] L.D. Landau and E.M. Lifshitz, "On the theory of the dispersion of magnetic permeability in ferromagnetic bodies," Phys. Z. Sowjetunion **8**, 153 (1935).

[14] Thomas L Gilbert, "A phenomenological theory of damping in ferromagnetic materials," IEEE Trans. Magn. **40**, 3443–3449 (2004).

[15] D.A. Garanin, "Generalized equation of motion for a ferromagnet," Physica A **172**, 470 (1991).

[16] A Rebei and G.J. Parker, "Fluctuations and dissipation of coherent magnetization," Phys. Rev.B **67**, 104434 (2003).

[17] P. Nieves, D. Serantes, U. Atxitia, and O. Chubykalo-Fesenko, "Quantum landau-lifshitz-bloch equation and its comparison with the classical case," Phys. Rev. B **90**, 104428 (2014).

[18] Matthew OA Ellis, Richard FL Evans, Thomas A Ostler, Joseph Barker, U Atxitia, O Chubykalo-Fesenko, and Roy W Chantrell, "The Landau-Lifshitz equation in atomistic models," Low Temp. Phys. **41**, 705–712 (2015).

[19] Satadeep Bhattacharjee, Lars Nordstrom, and Jonas Fransson, "Atomistic spin dynamic method with both damping and moment of inertia effects included from first principles," Phys. Rev. Lett. **108**, 057204 (2012).

[20] Richard FL Evans, Weijia J Fan, Phanwadee Chureemart, Thomas A Ostler, Matthew OA Ellis, and Roy W Chantrell, "Atomistic spin model simulations of magnetic nanomaterials," J. Phys.: Condens. Matter **26**, 103202 (2014).

[21] B Dieny, I.L. Prejbeanu, K Garello, and *et al*, "Opportunities and challenges for spintronics in the microelectronics industry," Nature Electr. **3**, 446 (2020).

[22] David Beaujouan, Pascal Thibaudeau, and Cyrille Barreteau, "Anisotropic magnetic molecular dynamics of cobalt nanowires," Phys. Rev. B **86**, 174409 (2012).

[23] Pui-Wai Ma, C. H. Woo, and S. L. Dudarev, "Large-scale simulation of the spin-lattice dynamics in ferromagnetic iron," Phys. Rev. B **78**, 024434 (2008).

[24] Pui-Wai Ma and C. H. Woo, "Parallel algorithm for spin and spin-lattice dynamics simulations," Phys. Rev. E **79**, 046703 (2009).

[25] J. Tranchida, S.J. Plimpton, P. Thibaudeau, and A.P. Thompson, "Massively parallel symplectic algorithm for coupled magnetic spin dynamics and molecular dynamics," J. Comput. Phys. **372**, 406 – 425 (2018).

[26] Dilina Perera, Markus Eisenbach, D. M. Nicholson, G. M. Stocks, and D. P. Landau, "Reinventing atomistic magnetic simulations with spin-orbit coupling," Phys. Rev. B **93**, 060402(R) (2016).

[27] Matthias Aßmann and Ulrich Nowak, "Spin-lattice relaxation beyond gilbert damping," J. Magn. Magn. Mater **469**, 217 – 223 (2019).

[28] Johan Hellsvik, Danny Thonig, Klas Modin, Diana Iusan, Anders Bergman, Olle Eriksson, Lars Bergqvist, and Anna Delin, "General method for atomistic spin-lattice dynamics with first-principles accuracy," Phys. Rev. B **99**, 104302 (2019).

[29] S. Karakurt, R.W. Chantrell, and U. Nowak, "A model of damping due to spin–lattice interaction," J. Magn. Magn. Mater **316**, e280 – e282 (2007).

[30] J. Fransson, D. Thonig, P. F. Bessarab, S. Bhattacharjee, J. Hellsvik, and L. Nordstrom, "Microscopic theory for coupled atomistic magnetization and lattice dynamics," Phys. Rev. Materials **1**, 074404 (2017).

[31] Marco Di Gennaro, Alonso L. Miranda, Thomas A. Ostler, Aldo H. Romero, and Matthieu J. Verstraete, "Competition of lattice and spin excitations in the temperature dependence of spin-wave properties," Phys. Rev. B **97**, 214417 (2018).

[32] Pui-Wai Ma, S. L. Dudarev, and C. H. Woo, "Spin-lattice-electron dynamics simulations of magnetic materials," Phys. Rev.

B **85**, 184301 (2012).

33 Pui-Wai Ma, S. L. Dudarev, and Jan S. Wróbel, "Dynamic simulation of structural phase transitions in magnetic iron," Phys. Rev. B **96**, 094418 (2017).

34 Pui-Wai Ma and S. L. Dudarev, "Longitudinal magnetic fluctuations in langevin spin dynamics," Phys. Rev. B **86**, 054416 (2012).

35 A. V. Ruban, S. Khmelevskyi, P. Mohn, and B. Johansson, "Temperature-induced longitudinal spin fluctuations in fe and ni," Phys. Rev. B **75**, 054402 (2007).

36 Louis A Girifalco and Victor G Weizer, "Application of the Morse potential function to cubic metals," Phys. Rev. **114**, 687 (1959).

37 VJ Minkiewicz, G Shirane, and R Nathans, "Phonon dispersion relation for iron," Phys. Rev. **162**, 528 (1967).

38 Matthew Ellis, *Simulations of magnetic reversal properties in granular recording media*, Ph.D. thesis, University of York (2015).

39 SL Dudarev and PM Derlet, "A 'magnetic'interatomic potential for molecular dynamics simulations," J. Phys. Condens. Matter **17**, 7097 (2005).

40 Peter M Derlet and SL Dudarev, "Million-atom molecular dynamics simulations of magnetic iron," Prog. Mater. Sci. **52**, 299–318 (2007).

41 Pui-Wai Ma and S. L. Dudarev, "Atomistic spin-lattice dynamics," in *Handbook of Materials Modeling: Methods: Theory and Modeling*, edited by Wanda Andreoni and Sidney Yip (Springer International Publishing, Cham, 2020) pp. 1017–1035.

42 J. H. Van Vleck, "On the anisotropy of cubic ferromagnetic crystals," Phys. Rev. **52**, 1178–1198 (1937).

43 Aleksandr I Akhiezer, SV Peletminskii, and Victor G Baryakhtar, "Spin waves," (1968).

44 Markus Eisenbach, Donald M Nicholson, Aurelian Rusanu, and Greg Brown, "First principles calculation of finite temperature magnetism in fe and fe3c," Journal of Applied Physics **109**, 07E138 (2011).

45 Rep Kubo, "The fluctuation-dissipation theorem," Reports on progress in physics **29**, 255 (1966).

46 Oksana Chubykalo, Roman Smirnov-Rueda, JM Gonzalez, MA Wongsam, Roy W Chantrell, and Ulrich Nowak, "Brownian dynamics approach to interacting magnetic moments," J. Magn. Magn. Mater **266**, 28–35 (2003).

47 Olle Eriksson, Anders Bergman, Lars Bergqvist, and Johan Hellsvik, *Atomistic spin dynamics: Foundations and applications* (Oxford university press, 2017).

48 G. P. Muller, Markus Hoffmann, Constantin Disselkamp, Daniel Schurhoff, Stefanos Mavros, Moritz Sallermann, N. S. Kiselev, Hannes Jonsson, and Stefan Blugel, "Spirit: Multifunctional framework for atomistic spin simulations," Phys. Rev. B **99**, 224414 (2019).

49 F. Kormann, B. Grabowski, B. Dutta, T. Hickel, L. Mauger, B. Fultz, and J. Neugebauer, "Temperature dependent magnon-phonon coupling in bcc fe from theory and experiment," Phys. Rev. Lett. **113**, 165503 (2014).

50 Biswanath Dutta, Fritz Kormann, Subhradip Ghosh, Biplab Sanyal, Jörg Neugebauer, and Tilmann Hickel, "Phonons in magnetically disordered materials: Magnetic versus phononic time scales," Phys. Rev. B **101**, 094201 (2020).

51 Matthew Heine, Olle Hellman, and David Broido, "Effect of thermal lattice and magnetic disorder on phonons in bcc fe: A first-principles study," Phys. Rev. B **100**, 104304 (2019).

52 Masuo Suzuki, "Generalized Trotter's formula and systematic approximants of exponential operators and inner derivations with applications to many-body problems," Commun. Math. Phys. **51**, 183–190 (1976).

53 Shan-Ho Tsai, H. K. Lee, and D. P. Landau, "Molecular and spin dynamics simulations using modern integration methods," A. J. Phys. **73**, 615–624 (2005).

54 Shan-Ho Tsai, M. Krech, and D.P. Landau, "Symplectic integration methods in molecular and spin dynamics simulations," Braz. J. Phys. **34**, 384–391 (2004).

55 I.P. Omelyan, I.M. Mryglod, and R Folk, "Algorithm for molecular dynamics simulations of spin liquids," Phys. Rev. Lett. **86**, 898 (2001).

56 Debra Lewis and Nilima Nigam, "Geometric integration on spheres and some interesting applications," J. Comput. Appl. Math. **151**, 141–170 (2003).

57 Pui-Wai Ma, S. L. Dudarev, A. A. Semenov, and C. H. Woo, "Temperature for a dynamic spin ensemble," Phys. Rev. E **82**, 031111 (2010).

58 Richard Evans, Ulrich Nowak, Florian Dorfbauer, T Shrefl, Oleg Mryasov, Roy W Chantrell, and Gregory Grochola, "The influence of shape and structure on the Curie temperature of Fe and Co nanoparticles," J. Appl. Phys. **99**, 08G703 (2006).

59 G. Dos Santos, R. Aparicio, D. Linares, E. N. Miranda, J. Tranchida, G. M. Pastor, and E. M. Bringa, "Size- and temperature-dependent magnetization of iron nanoclusters," Phys. Rev. B **102**, 184426 (2020).

60 Charles Kittel, "Physical theory of ferromagnetic domains," Reviews of modern Physics **21**, 541 (1949).

61 Akashdeep Kamra, Hedyeh Keshtgar, Peng Yan, and Gerrit EW Bauer, "Coherent elastic excitation of spin waves," Phys. Rev. B **91**, 104409 (2015).

62 D. Sander, "The correlation between mechanical stress and magnetic anisotropy in ultrathin films," Rep. Prog. Phys. **62**, 809–858 (1999).

63 NI Papanicolaou, IE Lagaris, and GA Evangelakis, "Modification of phonon spectral densities of the (001) copper surface due to copper adatoms by molecular dynamics simulation," Surf. Sci. **337**, L819–L824 (1995).

64 M Krech, Alex Bunker, and DP Landau, "Fast spin dynamics algorithms for classical spin systems," Comput. Phys. Commun. **111**, 1–13 (1998).

65 Dilina Perera, D. M. Nicholson, M. Eisenbach, G. M. Stocks, and David P Landau, "Collective dynamics in atomistic models with coupled translational and spin degrees of freedom," Phys. Rev. B **95**, 014431 (2017).

66 C-K Loong, JM Carpenter, JW Lynn, RA Robinson, and HA Mook, "Neutron scattering study of the magnetic excitations in ferromagnetic iron at high energy transfers," Journal of applied physics **55**, 1895–1897 (1984).

67 U. Atxitia, D. Hinzke, O. Chubykalo-Fesenko, U. Nowak, H. Kachkachi, O. N. Mryasov, R. F. Evans, and R. W. Chantrell, "Multiscale modeling of magnetic materials: Temperature dependence of the exchange stiffness," Phys. Rev. B **82**, 134440 (2010).

68 O. Chubykalo-Fesenko, U. Nowak, R.W. Chantrell, and D. Garanin, "Dynamic approach for micromagnetics close to the curie temperature," Phys. Rev. B **74**, 094436 (2006).

69 M.O.A. Ellis, T.A. Ostler, and R. W. Chantrell, "Classical spin model of the relaxation dynamics of rare-earth doped permalloy," Phys. Rev. B **86**, 174418 (2012).

70 Mara Strungaru, Sergiu Ruta, Richard F.L. Evans, and Roy W. Chantrell, "Model of magnetic damping and anisotropy at elevated temperatures: Application to granular fept films," Phys. Rev. Applied **14**, 014077 (2020).

71 C.L. Jermain, S.V. Aradhya, N.D. Reynolds, R.A. Buhrman, J.T. Brangham, M.R. Page, P.C. Hammel, F.Y. Yang, and D.C. Ralph, "Increased low-temperature damping in yttrium iron garnet thin films," Phys. Rev. B **95**, 174411 (2017).

[72] H. Maier-Flaig, S. Klingler, C. Dubs, O. Surzhenko, R. Gross, M. Weiler, H. Huebl, and S. T. B. Goennenwein, "Temperature-dependent magnetic damping of yttrium iron garnet spheres," Phys. Rev. B **95**, 214423 (2017).

[73] T Kasuya and RC LeCraw, "Relaxation mechanisms in ferromagnetic resonance," Phys. Rev. Lett. **6**, 223 (1961).

[74] Matthew O A Ellis, Mario Galante, and Stefano Sanvito, "Role of longitudinal fluctuations in L10 FePt," Phys. Rev. B **100**, 214434 (2019).

[75] R. F. L. Evans, U. Atxitia, and R. W. Chantrell, "Quantitative simulation of temperature-dependent magnetization dynamics and equilibrium properties of elemental ferromagnets," Phys. Rev. B **91**, 144425 (2015).

[76] Joseph Barker and G. E. W. Bauer, "Semiquantum thermodynamics of complex ferrimagnets," Phys. Rev. B **100**, 140401(R) (2019).

[77] A Ruckriegel and R.A. Duine, "Long-range phonon spin transport in ferromagnet–nonmagnetic insulator heterostructures," Phys.Rev.Lett. **124**, 117201 (2020).